Original Research

Discrimination of Axillary Metastatic from Nonmetastatic Lymph Nodes With PROPELLER Diffusion-Weighted MR Imaging in a Metastatic Breast Cancer Model and Its Correlation With Cellularity

Wang Junping, PhD,[1] Si Tongguo, PhD,[2] Zhang Yunting, PhD,[1]*
Yu Chunshui, PhD,[1] and Bai Renju, PhD[1]

Purpose: To assess the accuracy of apparent diffusion coefficient (ADC) in the differentiation of axillary metastatic from nonmetastatic lymph nodes in rabbits with metastatic breast cancer and to determine the relationship between the ADC and the cellularity of axillary lymph nodes of two different types.

Materials and Methods: The axillary lymph node models were created by inoculating VX2 cell suspensions in the mammary glands of 30 female rabbits. Conventional MR imaging and multi-shot fast-spin-echo PROPELLER DW imaging were performed approximately 4 weeks after successful inoculation. Images of axillary lymph nodes were analyzed with regard to size and ADC. Differences in the forementioned criteria between the two types of lymph nodes were assessed with reference to histopathologic findings. Cellularity was correlated with the ADC in all selected axillary lymph nodes.

Results: A total of 41 axillary metastatic and 29 inflammatory lymph nodes were successfully isolated. The size-based criteria showed no significant difference between the malignant and inflammatory lymph nodes (Ps > 0.05); however, the ADC of metastatic nodes was significantly lower than that of inflammatory nodes ($P < 0.001$). There was a significant inverse correlation between the ADC and cellularity ($r = -0.674$; $P < 0.001$) regardless of their different tissue types.

Conclusion: DW imaging is a new promising functional technique for differentiating metastatic from inflammatory lymph nodes. Furthermore, cellularity has a significant influence on the ADC in both malignant and benign lymph nodes.

Key Words: axillary lymph node; diffusion-weighted imaging; cell density; animal model
J. Magn. Reson. Imaging 2012;36:624–631.

BREAST CANCER is by far the most frequent malignancy among women throughout the world, and its incidence continues to increase (1). Axillary lymph node involvement is an essential prognostic factor and an important determinant in the treatment of patients with breast cancer (2,3). Metastatic breast cancer (MBC) is a special type of breast cancer and is usually associated with a very unfavorable prognosis. It has been confirmed that axillary lymph nodes are the most susceptible site of the metastatic cells' spread, which represent one of the most significant prognostic variables in MBC patients and are used to determine the need for adjuvant treatment. Current cross-sectional imaging modalities such as MR imaging, computed tomography, and ultrasonography rely on insensitive size and morphologic criteria and, thus, lack the desired accuracy for characterizing lymph nodes. This is mainly because metastases can be present in nonenlarged lymph nodes and not all enlarged nodes are malignant (4). Therefore, it has been concluded that lymph node size is not a reliable parameter for the evaluation of metastatic involvement. The low accuracy reported with size parameters prompted the evolution of imaging techniques from conventional anatomic modalities to molecular techniques in functional and physiologic assessment of lymph nodes.

Diffusion weighted (DW) imaging is a noninvasive functional MR imaging technique that shows tissue characteristics based on the molecular diffusion of

[1]Department of Radiology, Tianjin Medical University General Hospital, Tianjin, China.
[2]Department of Interventional Therapy, Tianjin Medical University Cancer Institute and Hospital; Key Laboratory of Cancer Prevention and Therapy, Tianjin, China.
Drs. Junping and Tongguo contributed equally to this work.
Contract grant sponsor: Science and Technology Fund of Tianjin Public Health Bureau, China; Contract grant number: 09KZ105.
*Address reprint requests to: Z.Y., Department of Radiology, Tianjin Medical University General Hospital, Anshan Road No. 154, Heping District, Tianjin 300052, China. E-mail: drzhangyt@163.com
Received August 6, 2011; Accepted April 11, 2012.
DOI 10.1002/jmri.23695
View this article online at wileyonlinelibrary.com.

water around cells, which is known as Brown motion (5,6).The apparent diffusion coefficient (ADC), which is derived from DW imaging and reflects the random thermal motion of protons, has been introduced to compare the diffusivity between lesions (7). It has become increasingly important in the assessment of malignant tumors, and it is now part of the standard imaging protocols for evaluation of the patients with breast cancer. Moreover, in recent years, the importance of ADC value has been reported in diagnosing benign and malignant lymph nodes in various regions (8–13). DW imaging can provide information on the biophysical properties of tissues such as cell organization, cell density, and microstructure (14). In general, the increased hypercellularity and nuclear-to-cytoplasmic (N/C) ratio, which are both frequently observed in malignancies, reduce the diffusion space of water protons in the extracellular and intracellular dimensions, with a resultant decrease in ADC value (15,16).

It is plausible that the cellularity of metastatic cancers in the nodes might not differ greatly from that in the primary lesions. The present study has extended these findings to show that the ADC assessment can also characterize axillary metastatic lymph nodes relative to nonmetastatic ones in the MBC model. Although DW imaging could find more lymph nodes than conventional anatomic sequences, it will be extremely difficult to assess pathology accurately comparing individual images. For patients with known nodal metastasis, biopsy rather than resectomy will be necessary for N staging, so that pathology diagnosis of each lymph node will be impossible. To determine the exact pathological result for each lymph node (node-by-node evaluation), we performed this study in which axillary metastatic and nonmetastatic lymph nodes were created by VX2 tumor MBC models to investigate the usefulness of the ADC value in characterizing the status of axillary lymph nodes and to assess the relationship between ADC and cellularity regardless of their different tissue types.

MATERIALS AND METHODS

Animal Preparation

Thirty female New Zealand White rabbits weighing 2.0 to 2.5 kg were allowed food and water ad libitum. The MBC model used was established as follows. Briefly, 1-mL suspensions containing 10^7 VX2 carcinoma cells (provided by Pathological Department of Peking Union Medical College, China) were extracted into a 1-mL syringe and injected into the rabbits' mammary gland, underneath the lateral upper quadrant of the bilateral second nipples. MR imaging was performed approximately 4 weeks after VX2 cell inoculation.

MR Protocol

MR imaging was conducted by using a 3.0 Tesla (T) scanner (HDx, GE Medical Systems, Milwaukee, WI) with a 3-inch animal surface coil covering the bilateral axilla regions to improve signal-noise-contrast. All animals were anesthetized with an intravenous injection of pentobarbitone and ketamine hydrochloride at 10–20 mg/4–5 mg per kilogram of body weight, respectively, to make sure that the breathing of each animal was slow and stable. They were placed head first in the prone position with adducted and elevated forepaws. After a localizer image of the axilla was obtained, the following sequences were performed: conventional T2W fast spin-echo in the axial and sagittal planes with or without fat suppression (TR/TE, 5000 ms/80 ms; matrix size, 320 × 224; FOV, 18 cm; number of excitation, 3; slice thickness, 3 mm; gap, 0.5 mm); T1-weighted spin-echo in transverse plane with or without fat suppression (TR/TE, 450 ms/30 ms; matrix size, 320 × 160; the remaining parameters were the same as T2W image).

Transverse DW imaging was obtained using a free-breath multi-shot fast-spin-echo PROPELLER (periodically rotated overlapping parallel lines with enhanced reconstruction) and ASSET (array spatial sensitivity encoding technique), with the following parameters: TR/TE, 4000 ms/60 ms; FOV, 18; matrix size, 224 × 128, ETL = 16; slice thickness, 3 mm; gap, 0.5 mm; 60 segments, nonselective fat saturation; acceleration factor for the parallel imaging, 2.5; b-value, 0 and 1000 s/mm^2. The DW gradients were applied in all three orthogonal directions, which were coincident with the slice-selective, phase-encoding, and readout directions of the gradient. The scanning time of DW imaging was 7 min 20 s.

Measurements of the Size and ADC Value of the Selected Axillary Lymph Nodes

All MR images were assessed with an emphasis placed on the bilateral axillary lymph nodes. No attention was paid to the stage of the MBC model. As small lymph nodes do not allow reliable identification and measurements, our study included only axillary lymph nodes with short-axis diameter of 5 mm or greater on axial T2W imaging. All the MR images were analyzed by consensus between two experienced radiologists who were blinded to the histological findings. The long- and short-axis diameters and the ADC value of the finally selected lymph nodes were measured at a workstation (ADW 4.3. GE Healthcare). The diameters were measured using the transverse plane on T2W images that contained the maximal area of the each lymph node. The greatest dimension of each evaluated lymph node was measured and defined as the long-axis diameter (L), and the greatest dimension perpendicular to L was measured and defined as the short-axis diameter (S). Then the L/S ratio was calculated. The ADC maps were calculated on a pixel-by-pixel basis by using built-in software (ADW 4.3. GE Healthcare). Also the corresponding central slice of each lymph node on the ADC map, a round or elliptical region of interest (ROI) covering approximately 3/4 of the entire area of the selected lymph node was used, while attempting to avoid inclusion of the margins, whereas T2W imaging was used to the anatomical reference. The area of the ROI in lymph nodes was 30–100 mm^2 according to their different sizes. All the

measurements obtained from the two readers were averaged and were expressed as means ± standard deviations.

Histological Evaluation and Determination of Cellularity

After MR examination, all rabbits were killed immediately by air injection into the auriborder vein. The targeted axillary lymph nodes were carefully removed according to the MR images, labeled for orientation and location, and were then fixed in 10% neutral formalin followed by routine paraffin imbedding to prepare 4-μm-thick sections with hematoxylin–eosin (HE) staining, which was used to assess the lymph node morphology. Each specimen was sliced transversely at 3-mm intervals. The slice and location of each selected axillary lymph node were matched with the corresponding axial T2W images to enable a node-for-node comparison of MR images and histological findings. The final pathological result was determined according to the characteristic of cellular structure observed under an optic microscope (Olympus, BX 50, Japan).

Cellularity analysis was performed on a computer-based image analysis software (NIS-Elements, Nikon, Japan) connected to the above optic microscope (original magnification, ×400). Cellularity was defined as the total area of nuclei of cells divided by the area of the whole histological section. Five fields of each histological specimen were chosen randomly to include as many cells as possible. The mean of five fields was taken as the cellularity, also expressed as means ± standard deviations.

Statistical Analysis

Statistical analysis was performed using Statistical Package for Social Science software (SPSS, version 18.0). Kolmogorov-Smirnov distances were considered to determine whether the size, ADC value, or cellularity was normally distributed. Because of equal variances, a Student's t-test was used to compare the size, ADC value, and cellularity, respectively, in the axillary metastatic and nonmetastatic lymph nodes with reference to the corresponding histologically determined nodal status as the standard. The Pearson's correlation coefficient was obtained to compare the ADC value and cellularity. In every statistical analysis, significance was considered when the P value was less than 0.05. To evaluate the diagnostic performance of the ADC value in distinguishing the axillary metastatic from nonmetastatic lymph nodes, a receiver-operating-characteristics (ROC) curve analysis was performed. Thereafter, the areas-under-the-curve (Az) were evaluated. From the ROC curve, the optimal cut-off value, which showed the best-performance (minimal false-negative and false-positive results) between the malignant and benign lymph nodes, was extracted. Sensitivity, specificity, positive predictive value (PPV), negative predictive value (NPV), and overall accuracy were calculated.

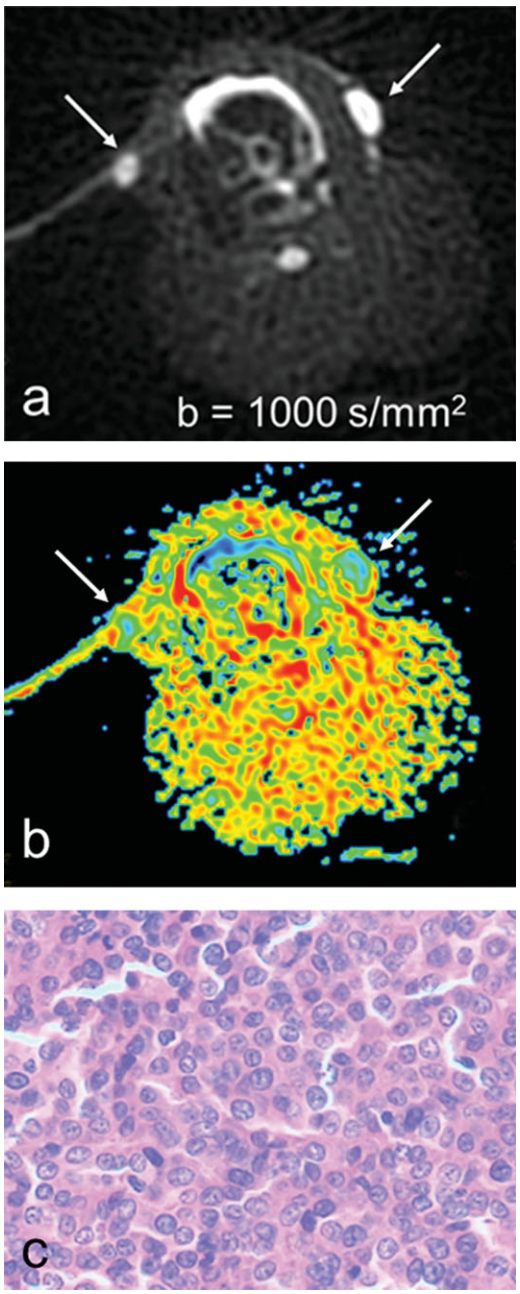

Figure 1. Two metastatic lymph nodes in the bilateral axillae. **a**: Axial DW imaging. Both axillary metastatic lymph nodes show obviously homogeneous hyperintensity with clear margin (arrow). **b**: The corresponding ADC map. The ADC value of the two nodes (arrow) is 0.654×10^{-3} mm^2/s and 0.621×10^{-3} mm^2/s, respectively. **c**: Histopathological examination (hematoxylin–eosin stain (HE); original magnification, ×400) shows that tumor cells are deposited within the left axillary metastatic lymph node, and enlarged nuclei, high N/C ratio, and pathological mitotic figures are observed. These findings confirm a dense cellular tumor with cellularity of 53%.

RESULTS

Histopathologic Findings

Seventy axillary lymph nodes with the short-diameter equal or greater than 5 mm were isolated by correlating MR images with pathological findings, including

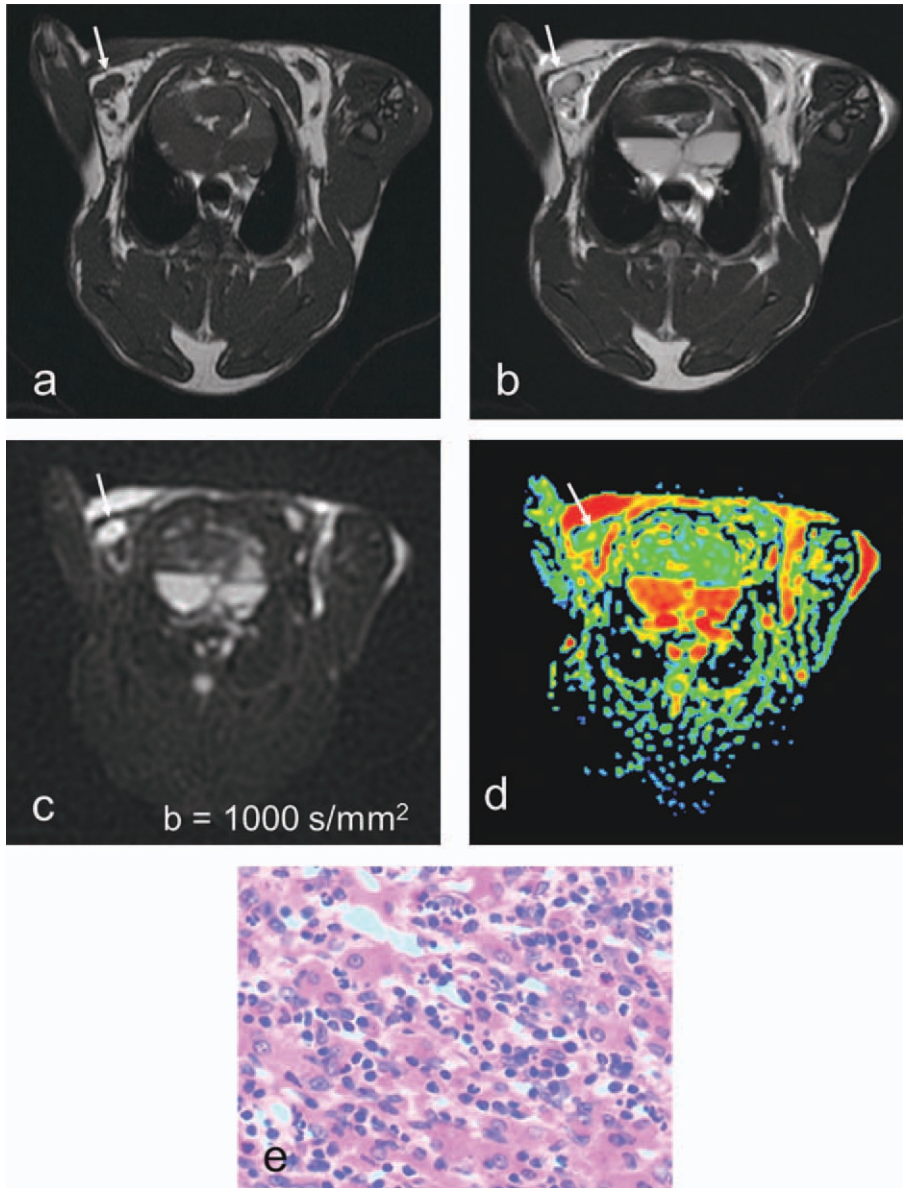

Figure 2. An inflammatory lymph node in the right axillary fossa. **a**: Axial T1W imaging. The inflammatory lymph node in the right axillary region shows isointensity with a clear borderline (arrow). **b**: Axial T2W imaging. It shows high signal intensity (arrow). **c**: The corresponding DW image demonstrates homogeneous high signal intensity (arrow). **d**: The corresponding ADC map. The node is depicted as an area of green in most part with yellow dots in the center (arrow). The ADC value of this node is 1.01×10^{-3} mm^2/s. **e**: Histopathological examination (hematoxylin–eosin (HE); original magnification, ×400) shows that abundant lymphocytes and plasmacytes infiltration were observed mainly in the nodes, with cell arrangement sparsely and with cellularity of 37%. [Color figure can be viewed in the online issue, which is available at wileyonlinelibrary.com.]

41 metastatic lymph nodes and 29 nonmetastatic lymph nodes (inflammatory reactive hyperplasia). In axillary metastatic lymph nodes, tumor metastasis resulted in destruction of the lymph nodes, where numerous densely stained tumor cells with large nuclei could be found. The cancer cells were large in size, round or ovoid in shape, showing increased N/C ratio, and cells with multiple nucleoli and pathological division could be seen. These features are consistent with moderately differentiated squamous cell carcinoma (Fig. 1). In axillary inflammatory reactive hyperplastic lymph nodes, abundant lymphocyte and plasmacyte infiltration, reactive hyperplasia, and fibrous connective tissue proliferation were observed mainly in the nodes (Fig. 2).

Imaging Analysis

When PROPELLER technique and ASSET were used, image distortion was significantly reduced to a minimum on the DW images, no obvious motion artifacts were present, and all the images were of diagnostic quality. All of the finally selected axillary lymph nodes appeared as oval- or round-shaped structures with isointensity relative to the adjacent skeletal muscle on T1W images, and hyperintensity on both T2W images and DW images (Figs. 1, 2). Comparison of L, S, L/S ratio, and the ADC values between metastatic and nonmetastatic lymph nodes by the Student's t-test showed that the L and S values of axillary metastatic lymph nodes were larger than those of the nonmetastatic lymph nodes, respectively; the L/S ratio was smaller in metastatic than nonmetastatic lymph nodes, however, the difference of each size-based criteria was not statistically significant (Ps > 0.05); whereas the ADC value was significantly lower for metastatic lymph nodes than for the nonmetastatic ones ($P < 0.001$) (Figs. 1, 2). The comparison of the measurements in lymph nodes of two groups is shown in Table 1. From the ROC curve (Fig. 3), when an ADC value of 1.04×10^{-3} mm^2/s was determined as a cutoff value for differentiating metastatic from

Table 1
Comparison of Sizes and ADC Values Between the Axillary Metastatic and Nonmetastatic Lymph Nodes

Variables	Metastatic LNs	Nonmetastatic LNs	t value	*P* value
L (mm)	13.52±1.41	11.95±1.19	1.631	0.098
S (mm)	10.01±1.29	8.81±1.50	2.085	0.071
L/S ratio	1.30±0.18	1.40±0.24	−1.592	0.101
ADC value ($\times 10^{-3} mm^2/s$)	0.878±0.224	1.241±0.185	−8.730	<0.001

LNs = lymph nodes.

nonmetastatic lymph nodes, where Youden index reached peak, the Az is 0.937 (standard error, 0.026; 95% CI, 0.886–0.988) and the sensitivity, specificity, PPV, NPV, and overall accuracy would be 93% (38/41), 93% (27/29), 95% (38/40), 90%(27/30), and 93% (65/70), respectively.

Relationship Between Cellularity and ADC Value

The cellularity of axillary metastatic and nonmetastatic lymph nodes was 50.01% ± 10.26% and 35.34% ± 11.82%, respectively, with significant difference = 7.895 ($P < 0.001$). There was a significantly inverse correlation between the ADC value and cellularity ($r = -0.674$; $P < 0.001$) of the axillary lymph nodes regardless of their different tissue types. The scatter plot shows that cellularity was higher in axillary metastatic lymph nodes that had lower ADC than nonmetastatic lymph nodes, and vice versa (Fig. 4).

DISCUSSION

VX2 tumor cell line is a moderately differentiated squamous carcinoma cell line that is induced by the Shope virus and develops after 72 times or more transfer of culture (17). It is implanted easily and grows quickly so that the diameter of the tumor can reach 2 cm in 3 or more weeks after implantation. VX2 tumors show a high potential for metastasizing to the regional lymph nodes and distant sites such as the lungs, liver, and bone (18). In the present study, the MBC model was successfully established in female animals by injecting a VX2 tumor cell suspension into the mammary gland of rabbit. Histopathologic examination 4 weeks after successful implantation revealed that the VX2 tumor had metastasized to axillary lymph nodes in 58.57% (41/70) of the rabbits, which might provide us with an opportunity to perform experiments relevant to lymph node metastasis. All these characteristics are quite similar to the human MBC model, so this model could be used for assessing the diagnostic value of newly exploited imaging modalities in the identification and characterization of tumor metastasis. In this experiment, we only focused on the metastatic and nonmetastatic lymph nodes (inflammatory reactive hyperplasia) in the axilla. We injected VX2 carcinoma cell suspensions into the rabbits' mammary gland underneath the lateral upper quadrant of the bilateral second nipples to create as many as possible axillary metastatic lymph nodes. Almost 90% of axillary lymph nodes are sentinel lymph nodes (SLN), which are the nodes that first receive lymph from the area of the breast harboring tumor. If the SLN is determined to be free of disease,

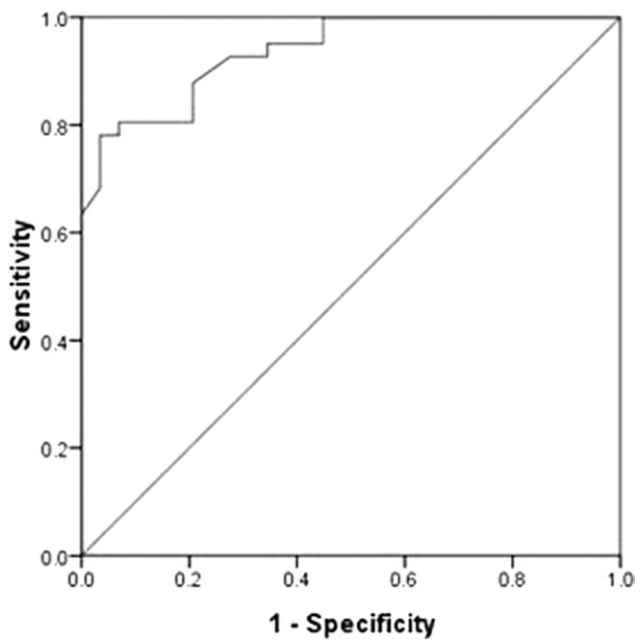

Figure 3. The ROC curve for the ADC value for differentiating the axillary inflammatory from metastatic lymph nodes. The AUC is 0.937.

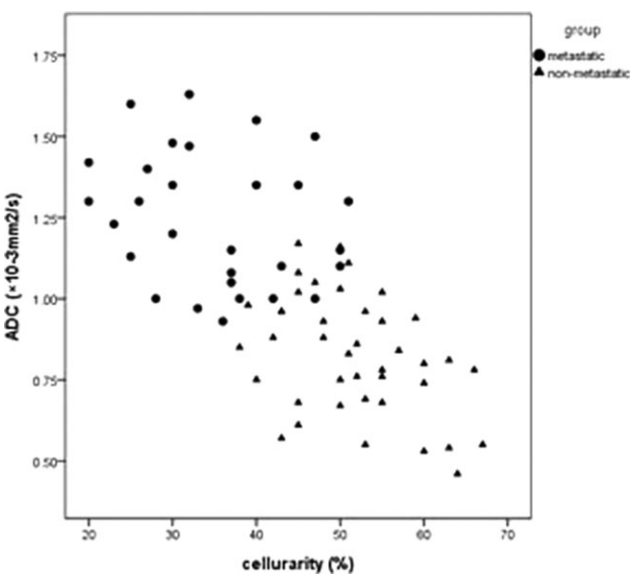

Figure 4. Relationship between cellularity and ADC value in axillary lymph nodes. There is a significant negative correlation ($r = -0.674$; $P < 0.001$), regardless of metastases.

it is assumed that all other regional lymph nodes will be negative and axillary dissection can be avoided.

Current imaging techniques rely heavily on the size criterion for characterization of nodal disease. A threshold diameter of 10 mm in the short axis was usually applied for differentiating metastatic from nonmetastatic lymph nodes, however, with relatively low sensitivity and specificity (4,19,20). Obwegeser et al (21) reported that, in histological analysis of 1249 axillary lymph nodes in 71 patients with breast cancer, 13.7% of metastatic nodes were 5–9 mm in short-axis diameter. Moreover, in a study of 4043 axillary lymph nodes in the setting of breast cancer, the use of a short-axis diameter of >10 mm plus a long-to-short axis ratio of <1.6 resulted in a sensitivity of 79% and a specificity of 93% for the detection of lymph node metastasis, with nearly all false-negative axillae demonstrating metastatic lymph nodes measuring < 10 mm (22). In our study, among 41 axillary metastatic lymph nodes, only 18 nodes were larger than 10 mm in short-axis diameter, accounting for only 44%. So further imaging methods should be developed to improve the diagnostic accuracy.

DW imaging is currently the only functional imaging method to investigate diffusion activities of water molecules in vivo, which is an important MR imaging technique that enables the radiologist to move from morphological to functional assessment of diseases (23,24). However, conventional single-shot echo-planar-imaging (SS-EPI) approaches often result in relatively poor overall image quality due to geometric distortion, chemical shift artifacts, and limited spatial resolution, particularly for thoracic applications (25). One way to achieve distortion-free DW images is to use a periodically rotated overlapping parallel lines with enhanced reconstruction (PROPELLER) fast spin-echo (FSE) technique, which oversamples at the center of *k*-space and obtains inherent "navigator" information, for in-plane displacement and rotation (26,27). Our experimental results on a 3.0T MR system showed that the PROPELLER FSE approaches exhibit substantially reduced geometric distortions compared with SS-EPI, as demonstrated in Figure 5, provide DW images with high resolution, high signal-to-noise ratio, and better anatomic structure display, none of the DW images had major artifacts that warranted their exclusion from our study.

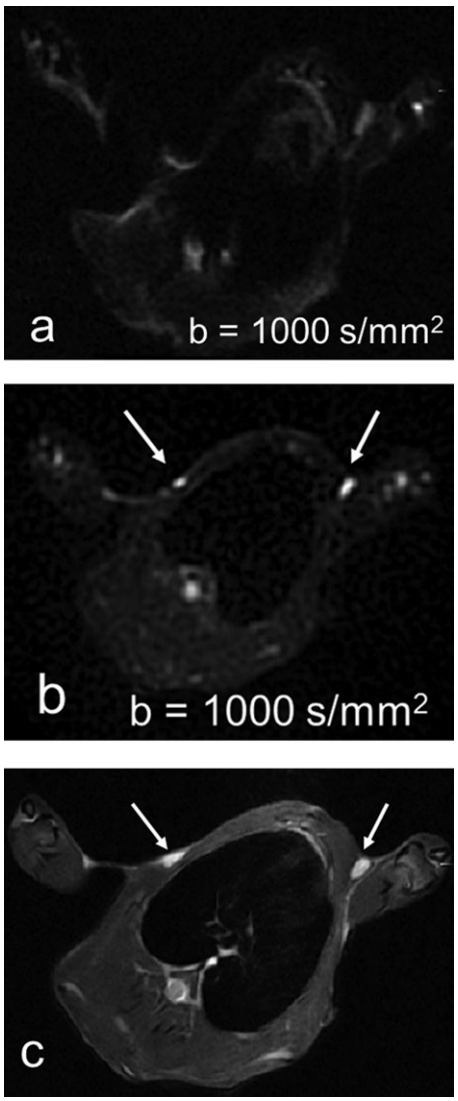

Figure 5. Axial DW images of the axillary fossa in a rabbit acquired using SS-EPI (**a**), PROPELLER FSE (**b**) techniques, and FSE T2W imaging (**c**). The geometric distortion of the whole image was so severe that the enlarged bilateral axillary lymph nodes were invisible on SS-EPI DW imaging (a). The distortion was substantially reduced in the image using the PROPELLER FSE approach, the resulting imaging shown in (b, arrow). It exhibits a nearly identical shape compared with the FSE T2W imaging in (c, arrow).

Because background tissue is usually suppressed on the native DW images, the conspicuity of small lymph nodes is markedly improved compared with the conspicuity of these nodes at conventional sequences. The improved conspicuity enables the depiction of these small nodes and the subsequent delineation of ROI. However, because both benign and malignant lymph nodes are hyperintense, visual assessment of DW images to differentiate them was a rather difficult task, as shown in Figures 1 and 2, so the measurement of ADC value is required for nodal characterization and it reflects the signal loss on DW images that occurs with increasing b-value. DW imaging simultaneously provides information on diffusion and perfusion (5,28). With a high value, the effect of perfusion is largely cancelled out; therefore, to evaluate the true diffusion of metastatic lymph nodes, our study applied a relatively high b-value, ie, 1000 s/mm^2.

DW imaging has been shown to enable differentiation between malignant and benign lymph nodes with sensitivities ranging from 83% to 93% and specificities ranging from 81% to 99%, albeit with different ADC thresholds (7,29,30). In this study, we evaluated the usefulness of DW imaging in discriminating axillary metastatic lymph nodes from nonmetastatic lymph nodes in MBC model, our finding showed the ADC value of the former was significantly lower than that of the latter, in good agreement with the results of prior investigators (7,29,30). Our ROC analysis showed satisfactory diagnostic performance of the

ADC value for differentiating the metastatic from the nonmetastatic lymph nodes, as the Az was 0.937. When the ADC value lower than 1.04 $\times 10^{-3}$ mm^2/s was used in determining metastatic lymph nodes, the resulting sensitivity, specificity, PPV, NPV, and overall accuracy were 93%, 93%, 95%, 90%, and 93%, respectively.

Cellularity, defined as the number of cells in a given area of tissue, was found to be an important factor that influences microscopic water diffusion, because it determines the extracellular space, while water diffusivity is greater in the extracellular space compared with that in the intracellular space (14–16). Therefore, an increase in cellularity, which would decrease the fraction of extracellular space, would result in restricted water diffusion. Malignancies are considered to commonly have denser cellularity than normal tissue and benign tumors, which relatively reduce the extracellular space, leading to restriction of the movement of water molecules. The diffusivity of water molecules in tissues is quantified by the ADC calculated from DW images. It is widely accepted that increased cell density causes reduced ADC. There are a few studies that have already described relationships between diffusion and cellular structure in cranial and extracranial tumors (14–16,31,32). Several groups have reported an inverse correlation of ADC with cell density in tumors (14–16).

ADC value, therefore, presents us with promising candidate biomarkers for the study of cellular structure. In our experiment, the cellularity of axillary metastatic lymph nodes was significantly denser than that of nonmetastatic lymph nodes and there is a significantly inverse correlation between the ADC value and cellularity regardless of their different tissue types. To the best of our knowledge, we present the first strong evidence that ADC also correlated with cellularity in lymph nodes. The lower ADC value observed in axillary metastatic lymph nodes could be explained by the histopathological manifestation of the resected specimen. In metastatic lymph nodes, tumor tissue invasion could be seen, the densely packed cancerous cells restricting extracellular diffusion of water protons; meanwhile, the N/C ratio of squamous cells is also a minor determinant of ADC values, which limits intracellular motion. So the dense cellularity combined with the high N/C ratio of metastatic lymph nodes led to a significant reduction in the ADC value.

However, certain overlap in cellular density among tumor metastasis and reactive hyperplasia in lymph nodes may have resulted in misclassification. Maybe there were two plausible explanations for this slight overlap. On the one hand, we found that not all of the metastatic lymph nodes were entirely replaced by cancer cells, some of them were partially replaced by cancer cells, resulting in metastatic areas with lower ADC and nonmetastatic areas with higher ADC. On the other hand, in inflammatory lymph nodes, inflammatory cell infiltration, reactive hyperplasia, and fibrous connective tissue proliferation could be seen, which also would limit the diffusion of water molecules, resulting in a moderate decrease in ADC.

There are some limitations in our study. First, as described previously, our study only contained axillary lymph nodes with a short diameter of 5 mm or greater, because ADC measurements on smaller nodes would be limited due to relatively low spatial resolution on DW imaging. Second, contrast-enhanced MR scanning should be performed to help discriminate necrotic or cystic degeneration and to compare methods, although most of the targeted axillary lymph nodes are homogeneous. Third, there were some difficulties in coinciding the exact site of the examined pathological specimen with the site of the ADC measurements, despite the great effort made to make directly compare between specific lymph nodes detected by MR imaging and by histopathology.

In conclusion, this preliminary experiment indicates that DW imaging is a simple and readily available noninvasive technique to distinguish metastatic from nonmetastatic lymph nodes in the axillary fossa in rabbits of the MBC model on the basis of cellularity, which represents an indirect indicator of the complexity of intercellular spaces and junctions, i.e., the histological architecture. DW imaging should be introduced in clinical practice as an integration of standard MR protocols used for patients with breast cancer to more accurately predict the status of axillary lymph nodes preoperatively.

REFERENCES

1. Wang L, Yao Q, Wang J, et al. MRI and hybrid PET/CT for monitoring tumor metastasis in a metastatic breast cancer model in rabbit. Nucl Med Commun 2008;29:137–143.
2. Orel SG, Schnall MD. MR imaging of the breast for the detection, diagnosis, and staging of breast cancer. Radiology 2001;220: 13–30.
3. Stets C, Brandt S, Wallis F, Buchmann J, Gilbert FJ, Heywang-Kobrunner SH. Axillary lymph node metastases: a statistical analysis of various parameters in MRI with USPIO. J Magn Reson Imaging 2002;16:60–68.
4. Torabi M, Aquino SL, Harisinghani MG. Current concepts in lymph node imaging. J Nucl Med 2004;45:1509–1518.
5. Park SO, Kim JK, Kim KA, et al. Relative apparent diffusion coefficient: determination of reference site and validation of benefit for detecting metastatic lymph nodes in uterine cervical cancer. J Magn Reson Imaging 2009;29:383–390.
6. Yasui O, Sato M, Kamada A. Diffusion-weighted imaging in the detection of lymph node metastasis in colorectal cancer. Tohoku J Exp Med 2009;218:177–183.
7. Lin G, Ho KC, Wang JJ, et al. Detection of lymph node metastasis in cervical and uterine cancers by diffusion-weighted magnetic resonance imaging at 3T. J Magn Reson Imaging 2008;28: 128–135.
8. Rechichi G, Galimberti S, Signorelli M, et al. Endometrial cancer: correlation of apparent diffusion coefficient with tumor grade, depth of myometrial invasion, and presence of lymph node metastases. AJR Am J Roentgenol 2011;197:256–262.
9. Roy C, Bierry G, Matau A, Bazille G, Pasquali R. Value of diffusion-weighted imaging to detect small malignant pelvic lymph nodes at 3 T. Eur Radiol 2010;20:1803–1811.
10. Nakayama J, Miyasaka K, Omatsu T, et al. Metastases in mediastinal and hilar lymph nodes in patients with non-small cell lung cancer: quantitative assessment with diffusion-weighted magnetic resonance imaging and apparent diffusion coefficient. J Comput Assist Tomogr 2010;34:1–8.
11. Eiber M, Beer AJ, Holzapfel K, et al. Preliminary results for characterization of pelvic lymph nodes in patients with prostate cancer by diffusion-weighted MR-imaging. Invest Radiol 2010;45: 15–23.

12. Chen YB, Liao J, Xie R, Chen GL, Chen G. Discrimination of metastatic from hyperplastic pelvic lymph nodes in patients with cervical cancer by diffusion-weighted magnetic resonance imaging. Abdom Imaging 2011;36:102–109.
13. Holzapfel K, Duetsch S, Fauser C, Eiber M, Rummeny EJ, Gaa J. Value of diffusion-weighted MR imaging in the differentiation between benign and malignant cervical lymph nodes. Eur J Radiol 2009;72:381–387.
14. Yamashita Y, Kumabe T, Higano S, Watanabe M, Tominaga T. Minimum apparent diffusion coefficient is significantly correlated with cellularity in medulloblastomas. Neurol Res 2009;31: 940–946.
15. Schnapauff D, Zeile M, Niederhagen MB, et al. Diffusion-weighted echo-planar magnetic resonance imaging for the assessment of tumor cellularity in patients with soft-tissue sarcomas. J Magn Reson Imaging 2009;29:1355–1359.
16. Zelhof B, Pickles M, Liney G, et al. Correlation of diffusion-weighted magnetic resonance data with cellularity in prostate cancer. BJU Int 2009;103:883–888.
17. Yuan YH, Xiao EH, Xiang J, et al. MR diffusion-weighted imaging of rabbit liver VX-2 tumor. World J Gastroenterol 2005;11: 3070–3074.
18. Geschwind JF, Artemov D, Abraham S, et al. Chemoembolization of liver tumor in a rabbit model: assessment of tumor cell death with diffusion-weighted MR imaging and histologic analysis. J Vasc Interv Radiol 2000;11:1245–1255.
19. Shetty MK, Carpenter WS. Sonographic evaluation of isolated abnormal axillary lymph nodes identified on mammograms. J Ultrasound Med 2004;23:63–71.
20. Krishnamurthy S, Sneige N, Bedi DG, et al. Role of ultrasound-guided fine-needle aspiration of indeterminate and suspicious axillary lymph nodes in the initial staging of breast carcinoma. Cancer 2002;95:982–988.
21. Obwegeser R, Lorenz K, Hohlagschwandtner M, Czerwenka K, Schneider B, Kubista E. Axillary lymph nodes in breast cancer: is size related to metastatic involvement? World J Surg 2000;24: 546–550.
22. Yoshimura G, Sakurai T, Oura S, et al. Evaluation of axillary lymph node status in breast cancer with MRI. Breast Cancer 1999;6:249–258.
23. Woodhams R, Ramadan S, Stanwell P, et al. Diffusion-weighted Imaging of the breast: principles and clinical applications. Radiographics 2011;31:1059–1084.
24. Usuda K, Zhao XT, Sagawa M, et al. Diffusion-weighted imaging is superior to positron emission tomography in the detection and nodal assessment of lung cancers. Ann Thorac Surg 2011;91:1689–1695.
25. Wang FN, Huang TY, Lin FH, et al. PROPELLER EPI: an MRI technique suitable for diffusion tensor imaging at high field strength with reduced geometric distortions. Magn Reson Med 2005;54:1232–1240.
26. Pipe JG. Motion correction with PROPELLER MRI: application to head motion and free-breathing cardiac imaging. Magn Reson Med 1999;42:963–969.
27. Deng J, Virmani S, Young J, et al. Diffusion-weighted PROPELLER MRI for quantitative assessment of liver tumor necrotic fraction and viable tumor volume in VX2 rabbits. J Magn Reson Imaging 2008;27:1069–1076.
28. Sumi M, Sakihama N, Sumi T, et al. Discrimination of metastatic cervical lymph nodes with diffusion-weighted MR imaging in patients with head and neck cancer. AJNR Am J Neuroradiol 2003;24:1627–1634.
29. Vandecaveye V, De Keyzer F, Vander Poorten V, et al. Head and neck squamous cell carcinoma: value of diffusion-weighted MR imaging for nodal staging. Radiology 2009;251:134–146.
30. Mizukami Y, Ueda S, Mizumoto A, et al. Diffusion-weighted magnetic resonance imaging for detecting lymph node metastasis of rectal cancer. World J Surg 2011;35:895–899.
31. Humphries PD, Sebire NJ, Siegel MJ, Olsen ØE. Tumors in pediatric patients at diffusion-weighted MR imaging: apparent diffusion coefficient and tumor cellularity. Radiology 2007;245:848–854.
32. Sadeghi N, D'Haene N, Decaestecker C, et al. Apparent diffusion coefficient and cerebral blood volume in brain gliomas: relation to tumor cell density and tumor microvessel density based on stereotactic biopsies. AJNR Am J Neuroradiol 2008;29:476–482.